J. Fluid Mech. (1991), *vol.* 224, *pp.* 29–47
Printed in Great Britain

The effect of jet injection geometry on two-dimensional momentumless wakes

By W. J. PARK[1] AND J. M. CIMBALA[2]

[1] Department of Nuclear and Energy Engineering, Cheju National University, Korea

[2] Mechanical Engineering Department, Pennsylvania State University, University Park, PA 16802, USA

(Received 6 October 1989 and in revised form 24 July 1990)

It is shown experimentally that a two-dimensional momentumless wake is strongly dependent on the jet injection configuration of the model. Namely, the decay rate of mean velocity overshoot ranged from $x^{-0.92}$ to $x^{-2.0}$ for three different configurations, while the spreading rate ranged from $x^{0.3}$ to $x^{0.46}$ for those same configurations. The magnitude of axial turbulence intensity was also found to depend on model configuration. On the other hand, the rate of decay of axial turbulence intensity was the same ($x^{-0.81}$) for all three models. In all cases the mean shear and Reynolds stress decayed rapidly, leaving nearly isotropic turbulence beyond 30 or 40 model diameters.

Appropriate length- and velocity scales are identified which normalize the mean velocity profiles into self-similar form. The shape of the normalized profile, however, was different for each configuration, indicating again that the initial conditions are felt very far downstream.

1. Introduction

Most elementary free-shear flows, such as wakes, jets, and mixing layers, are known to be asymptotically self-preserving; production and dissipation of turbulent energy are thus roughly in equilibrium. Although the relaxation length (i.e. the distance required to reach the fully developed state) depends on the geometry of the flow generator, the behaviour far downstream becomes independent of initial conditions (Narasimha & Prabhu 1972).

Momentumless wakes are produced by injection of fluid from the rear of a model such that the thrust exactly cancels the drag. For examples see Naudascher (1965) and Higuchi (1977) for axisymmetric geometry and Cimbala & Park (1990) for two-dimensional geometry. Momentumless wakes differ from elementary free-shear flows because the mean shear (and hence the production of turbulence) decays rapidly, causing a loss of balance between production and dissipation. It is expected therefore that momentumless far wakes may not be self-preserving, and may never become independent of initial conditions.

There have been several attempts to study the effect of initial conditions on axisymmetric momentumless wakes. Experimentally, Gran (1973), Schetz & Jakubowski (1975), and Higuchi (1977) observed such dependency for some flow quantities in axisymmetric momentumless wakes with different initial conditions. Finson (1975), utilizing a second-order-closure turbulence model, showed that numerically generated momentumless wakes also strongly depend on initial conditions. The primary objective of the present investigation was to study the effect of initial conditions on *two-dimensional* momentumless far wakes. The experiments

presented here are a direct follow-on to those reported in Cimbala & Park (1990). The reader is referred to that paper for details of the experimental set-up, and for an extensive literature review.

2. Experimental set-up

The present experiments were conducted in an open-return low-speed wind tunnel, the test section of which is 300×970 mm in cross-section and 2.4 m in length. Free-stream velocity was kept at 4.2 m/s for all cases, providing a Reynolds number of 5400 based on model diameter. To provide enough thrust to balance the model's drag, a controlled amount of air was injected through a slit (or multiple slits) at the base of the two-dimensional model. The present experiments are an extension of the authors' previous study (Cimbala & Park 1990); details of the experimental set-up can be found there and also in Park (1989).

Three types of two-dimensional air injection models were prepared: (*a*) a central single-jet injection model, (*b*) an asymmetric single-jet injection model and (*c*) a dual-jet injection model. The central single-jet injection model was chosen for investigation of the fundamental features of the two-dimensional momentumless wake (Cimbala & Park 1990). The other two injection models were modified from this basic model to produce momentumless wakes with different initial conditions by changing the geometry of momentum injection. For the dual-jet model, the last part of the air channel of the basic model was modified to produce two outer jets which are located symmetrically near the edges of the model. The asymmetric single-jet model was made simply by covering one of the dual-jet slits with thin tape. A diagram of the dual-jet injection model is shown in figure 1, while that of the central single-jet model was given in Cimbala & Park (1990). It is expected that the momentumless wake produced by the dual-jet injection model would be a two-dimensional counterpart of axisymmetric momentumless wakes produced by peripheral-jet or propeller-driven models. The asymmetric single-jet model was used to compare the difference, if any, between a symmetric and asymmetric momentumless wake.

3. Results

3.1. *Flow visualizations*

Smoke-wire flow visualizations were obtained for all three models along the centreline. Results for the smoke wire mounted at $x/d = 0$, 15, and 45 are shown in figures 2, 3, and 4 respectively. In figure 2, with the flow from 0 to 15 diameters visualized, the three momentumless wakes are compared. While the central single-jet model (*a*) contains only random features, a more organized flow pattern is observed for the other two cases. In the core region of the asymmetric momentumless wake (*b*) a wavy structure can be observed behind the trailing edge of the body. By analysing several photographs taken under conditions identical to those of (*b*), it was found that the streaklines are always initially skewed downward from the slit exit which is located at the upper edge of the model; the streaklines then meander along the centreline inside the wake boundaries forming a sinusoidal-wave-like structure thereafter. The flow field of the momentumless wake produced by the asymmetric single-jet model is thus strongly asymmetric about the centreline of the wake.

In the core region of the dual-jet momentumless wake (*c*) wavy structures similar to those of the asymmetric-jet model are also observed near the body. By careful

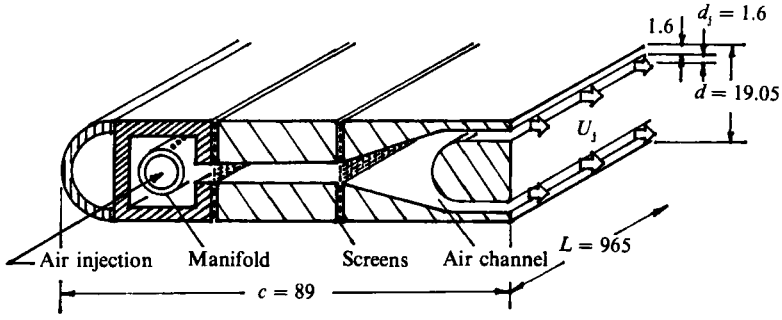

FIGURE 1. Two-dimensional momentumless-wake model: dual-jet injection model. Dimensions in mm.

examination of about 20 photographs of this flow field, it appears that the wake flaps up and down, apparently caused by the upper jet merging into the bottom jet and then vice versa. The flapping hypothesis was also supported by spectral analysis of hot-wire data (Park 1989). Namely, spectra for the dual-jet model contain a principal frequency plus harmonics, rather similar to the pure wake. It seems that Kármán vortex shedding, while suppressed for the central single-jet models and the asymmetric single-jet model, interacts with the dual jets of the third model, enhancing the observed flapping motion.

The widths of the momentumless wakes for all three cases very near the body are similar; however, the dual jet and the central single jet respectively become the widest and narrowest among the three cases.

In figure 3, the view is from 15–30 diameters, with the smoke wire mounted at $x/d = 15$. The asymmetric single-jet and dual-jet momentumless wakes (*b*) and (*c*) contain turbulent bursts similar to those of the central single-jet momentumless wake (*a*) as described in Cimbala & Park (1990). The wavy structures in the core regions of the asymmetric single-jet and dual-jet cases become disorganized at this downstream location.

In figure 4, the view is from 45–60 diameters. All three momentumless wakes become weaker and somewhat wider at these stations. While large structural motion for the central single-jet case (*a*) is substantially damped beyond 45 diameters downstream, more vigorous turbulence still remains in the asymmetric single-jet case (*b*) and the dual-jet case (*c*). Careful observation of (*b*) shows that the asymmetric single-jet momentumless wake contains a combination of jet-like patterns above and wake-like patterns below the centreline. In other words, the flow still contains both wake-like and jet-like characteristics locally, even though the net momentum deficit is zero. The dual-jet case (*c*), on the other hand, does not seem to have such structures locally; rather, the streakline pattern is more disorganized. These qualitative observations agree with the quantitative hot-wire measurements to be discussed next.

3.2. *Mean velocity profiles*

Velocity profile schematics for the momentumless wake are given with lengthscale definitions in figure 5. In particular, U_d is defined as the maximum velocity overshoot, $U_{max} - U_\infty$. Lengthscale l is defined as the half-width of the streamwise (axial) turbulence intensity. For elementary free-shear flows, the lengthscales based on the mean velocity profile and the turbulence intensity profile are essentially the same because of self-preservation. For the momentumless case, on the other hand,

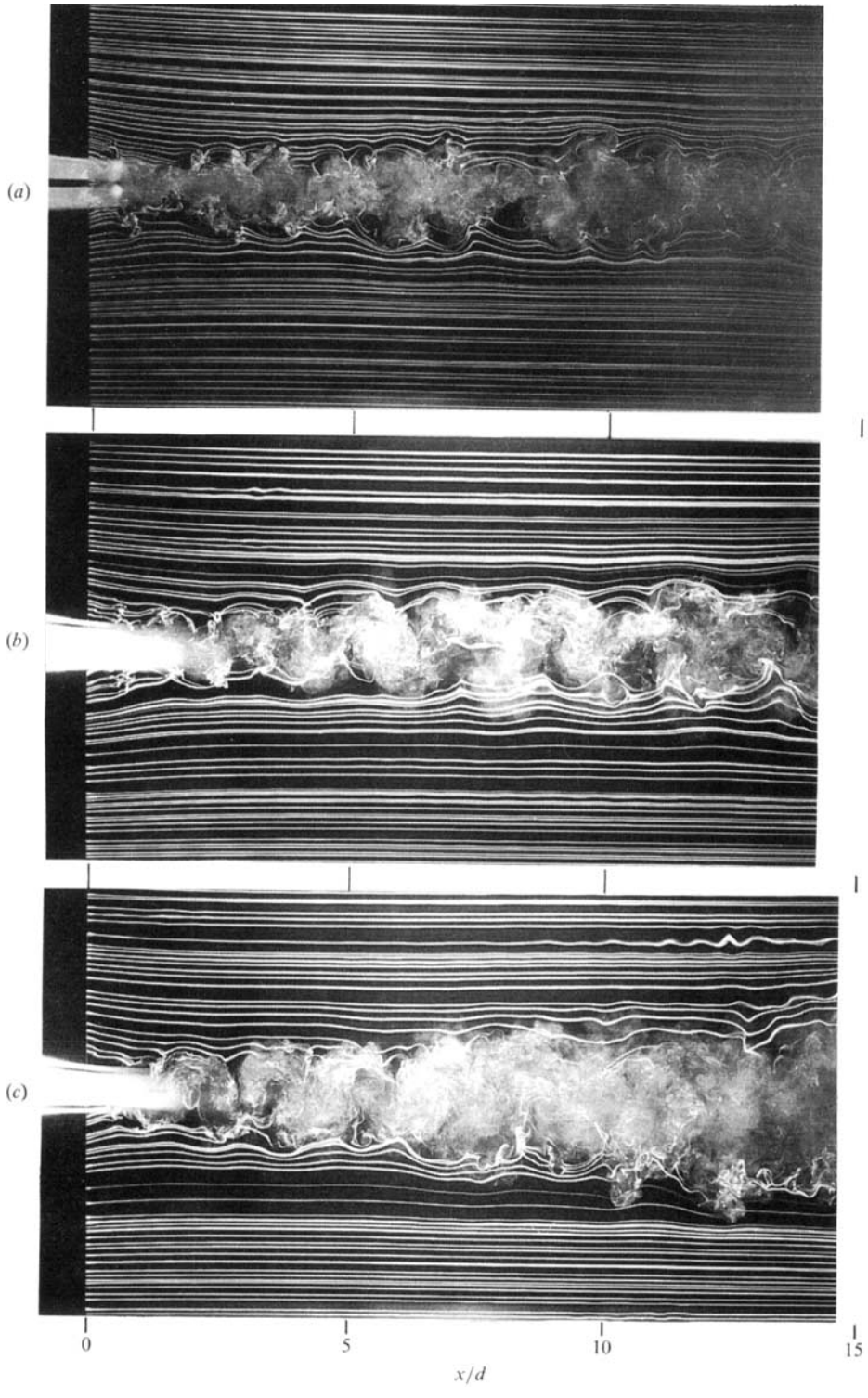

FIGURE 2. Flow visualization of momentumless wakes for three different models at $Re = 5400$, smoke-wire at $x/d = 0$: (*a*) central single-jet, (*b*) asymmetric single-jet and (*c*) dual-jet injection models.

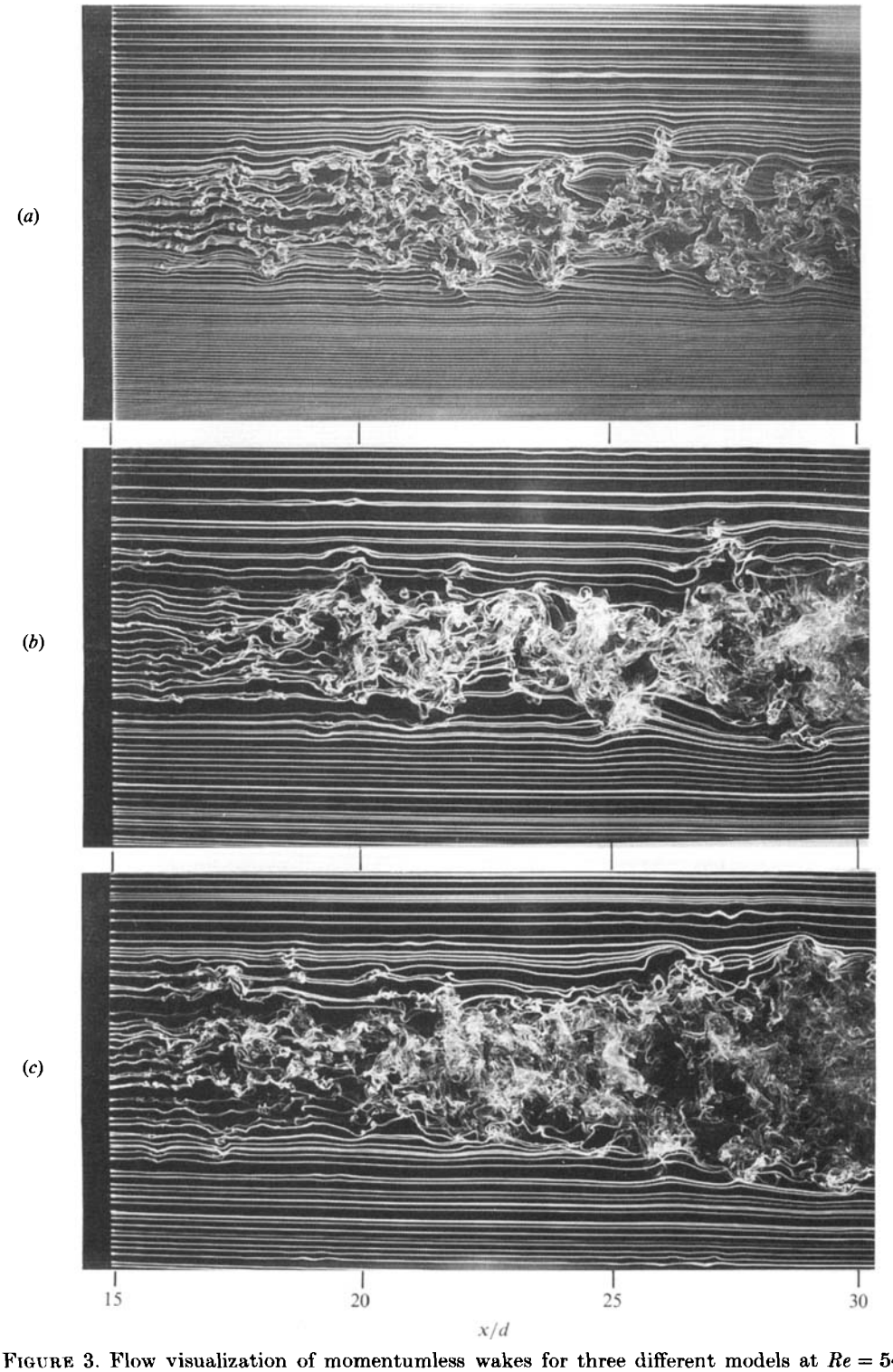

FIGURE 3. Flow visualization of momentumless wakes for three different models at $Re = 5400$, smoke-wire at $x/d = 15$: (*a*) central single-jet, (*b*) asymmetric single-jet and (*c*) dual-jet injection models.

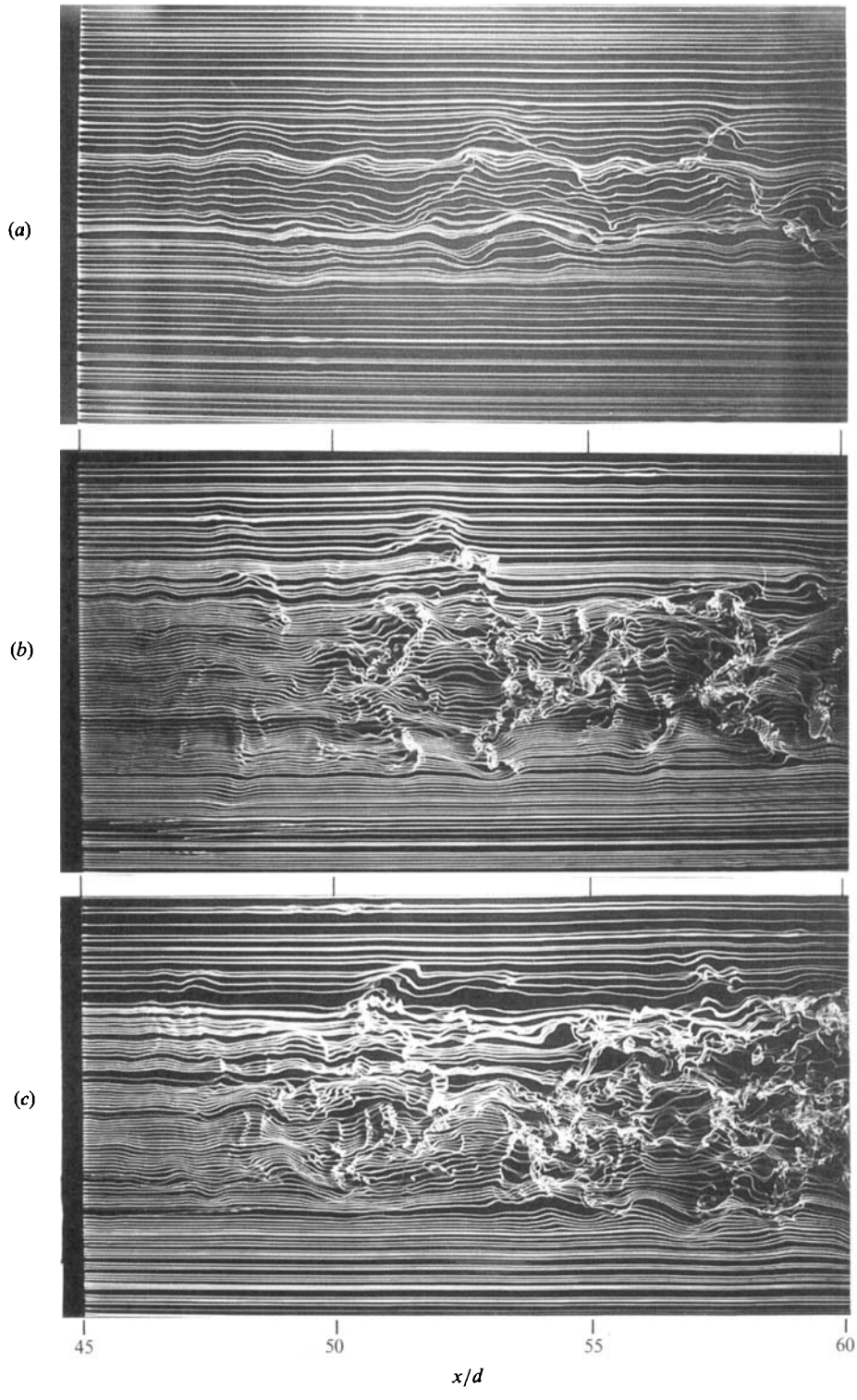

FIGURE 4. Flow visualization of momentumless wakes for three different models at $Re = 5400$, smoke-wire at $x/d = 45$: (*a*) central single-jet, (*b*) asymmetric single-jet and (*c*) dual-jet injection models.

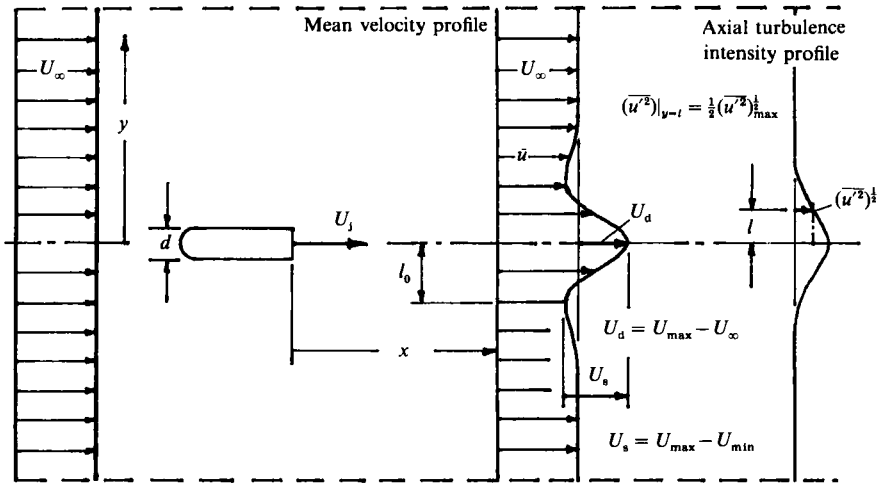

FIGURE 5. Velocity profile schematics, with lengthscale definitions.

these lengthscales may not coincide; therefore, another lengthscale based on the mean velocity profile, l_0, is defined as the distance between the transverse locations of the maximum and the minimum mean velocities. In addition, another mean velocity scale which is more general than U_d can be used to normalize various types of momentumless wakes; i.e. U_s, defined as the difference between the maximum and the minimum mean velocities.

To achieve momentumless states with the three injection models at fixed free-stream velocity, the momentum thickness,

$$\frac{\theta}{d} = \int_{-\infty}^{+\infty} \frac{\bar{u}}{U_\infty}\left(1 - \frac{\bar{u}}{U_\infty}\right) \mathrm{d}\left(\frac{y}{d}\right),$$

was calculated from the mean velocity profiles. By careful adjustment of the jet pressure, we were able to achieve near zero momentum; θ/d for all three momentumless wakes was less than 0.005 for all streamwise stations beyond 5 body diameters. The time-averaged mean velocity profiles were then measured at $Re_d = 5400$ for the three jet-injection cases at several downstream stations up to $x/d = 75$.

For all three momentumless wakes, the mean velocity profiles are normalized in two ways: (*a*) by the maximum velocity difference U_s and the lengthscale l_0 based on the mean velocity profile, and (*b*) by the maximum overshoot velocity U_d and the wake width l based on the turbulence intensity profile (see definition sketch in figure 5). Note that this latter normalization is the one adopted in previous studies of axisymmetric momentumless wakes.

For the central single-jet momentumless wake, the profiles with these two normalizations are plotted in figure 6(*a*, *b*) for $x/d = 5$ to 75. Although the magnitudes and the axial dependency of the two lengthscales are somewhat different, both normalizations are of similar quality for this case. This illustrates that lengthscale l may be broadly used to normalize mean flow as well as turbulent quantities. This is useful since the lengthscale l based on the turbulence intensity profile turns out to be more practical (i.e. easier to measure) than that based on the mean velocity profile, which quickly becomes flat beyond some distance downstream. Overall, the profiles normalized by either way are self-similar beyond $x/d = 5$.

The mean velocity profiles for the asymmetric single-jet case were measured for

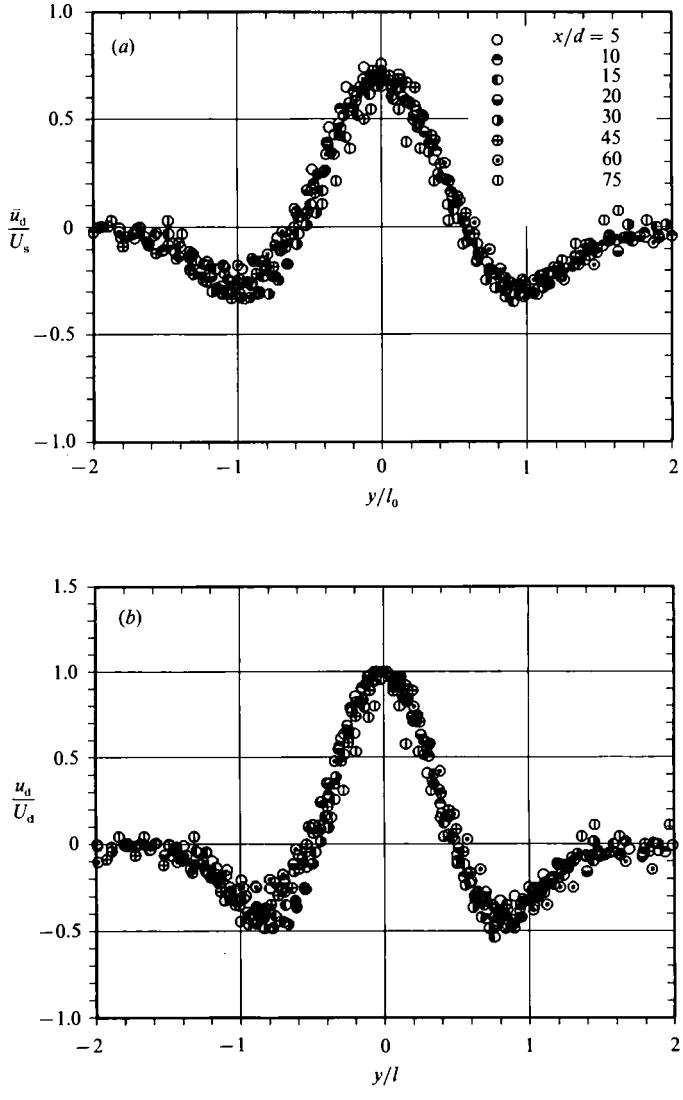

FIGURE 6. Normalized mean velocity profiles for the central single-jet momentumless wake at $Re = 5400$, $x/d = 5$ to 75: normalized by (*a*) l_0 and U_s, and (*b*) l and U_d.

$x/d = 1$ to 75. The asymmetric single-jet momentumless wake has a unique profile which seems to be patched with a jet-like profile at the upper half and a wake-like profile at the lower half of the flow field. In other words, the asymmetric single-jet momentumless wake maintains both wake and jet characteristics in a local sense, even though the whole flow field is momentumless from an integral point of view. These measurements are again consistent with our earlier smoke-wire observations (see figure 4*b*). The profiles normalized in two different ways for this case are presented in figure 7. Overall, the profiles normalized with U_s and l_0 (figure 7*a*) collapse better although there is some scatter in both cases.

For the case with U_s and l_0 (figure 7*a*), the maximum and minimum velocities in the non-dimensional profiles of the asymmetric single-jet momentumless wake occur at $y/l_0 \sim 0.375$ and $y/l_0 \sim -0.5$, respectively. The normalized asymmetric single-jet

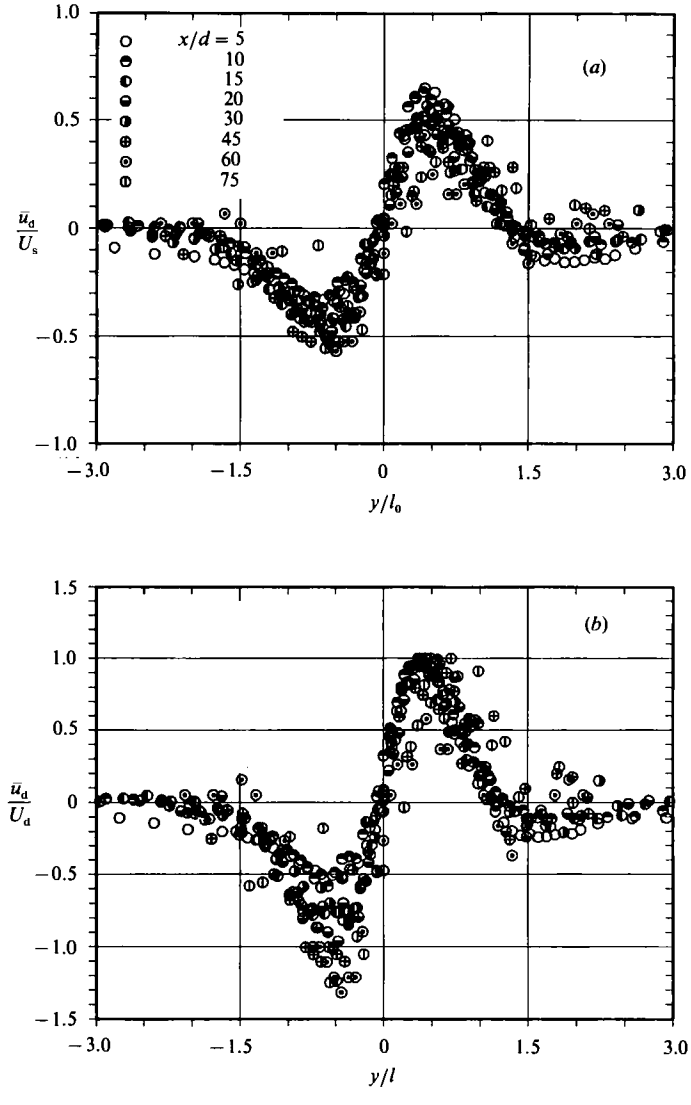

FIGURE 7. Normalized mean velocity profiles for the asymmetric single-jet momentumless wake at $Re = 5400$, $x/d = 5$ to 75: normalized by (*a*) l_0 and U_s, and (*b*) l and U_d.

momentumless wake profiles of figure 7 (*b*) collapse better on the jet-like side than on the wake-like side. Namely, the region of momentum defect in the non-dimensional profile becomes deeper as the axial distance increases. This means that the velocity scale U_s is more appropriate than U_d in the asymmetric single-jet momentumless wake because of the local characteristics discussed above. The peak velocity in the non-dimensional profiles in figure 7 (*b*) occurs again at $y/l \sim 0.375$; both lengthscales, l_0 and l turn out to be almost identical in the asymmetric single-jet momentumless wake. Note that the centreline of the jet slit is located at $y/d = 0.375$. Therefore, the normalized mean velocity profile of this type of momentumless wake flow is not independent of initial conditions and is rather closely related to the location of the initial jet injection slit off the centreline of the model. From the above point of view, this type of flow may better be labelled a *momentumless mixing layer*.

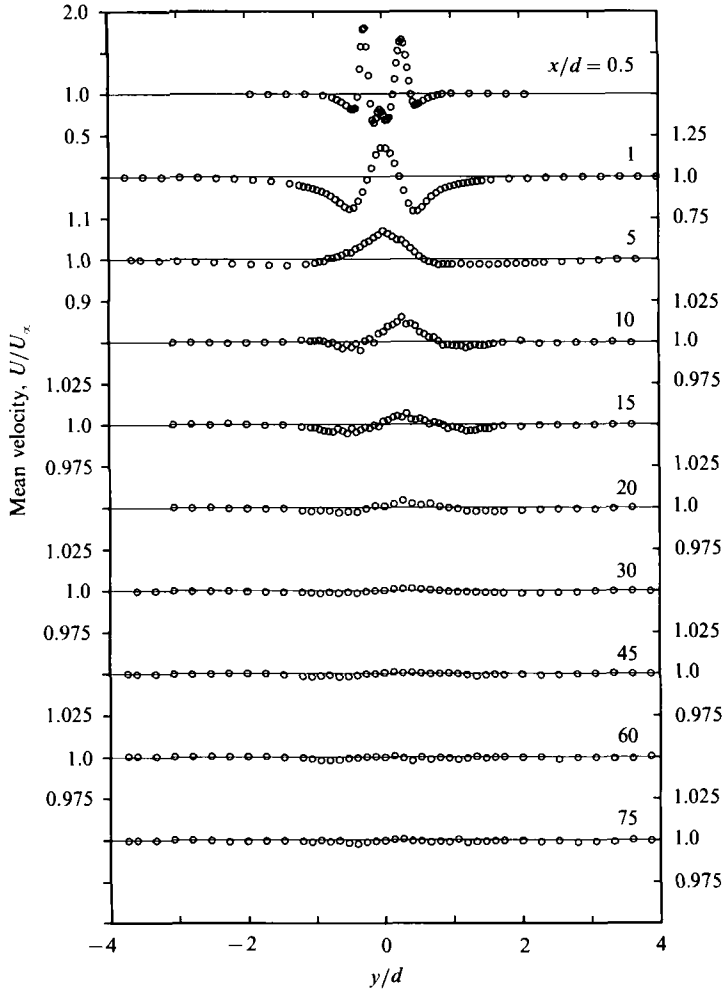

FIGURE 8. Mean velocity profiles for the momentumless wake at $Re = 5400$, at $x/d = 0.5$ to 75: the dual-jet model.

The mean velocity profiles for the dual-jet momentumless wake are presented consecutively along the flow direction in figure 8 for $x/d = 0.5$ to 75. At $x/d = 0.5$, dual peaks were observed in the mean velocity profile, corresponding to the two distinct jets. However, at $x/d = 1$ (which is equivalent to 12 jet slit widths downstream) the profile has a single peak similar to that of the central single-jet case. Furthermore, the profile is symmetric about the model centreline. This is due to the strong interaction between the dual jets; one jet merges into the other in an alternating manner and the resultant time-averaged mean velocity profile thus appears symmetric about the model centreline, even though instantaneously the flow field is highly unsymmetric. Vortices shed from the body may enhance this 'flapping' effect.

At $x/d = 5$, the peak of the dual-jet momentumless wake still occurs at the model centreline but its profile has a somewhat peculiar shape. By observing several other profiles of the dual-jet case at the same condition, the profile at this particular station was found to be strongly dependent on the averaging time of the measurements,

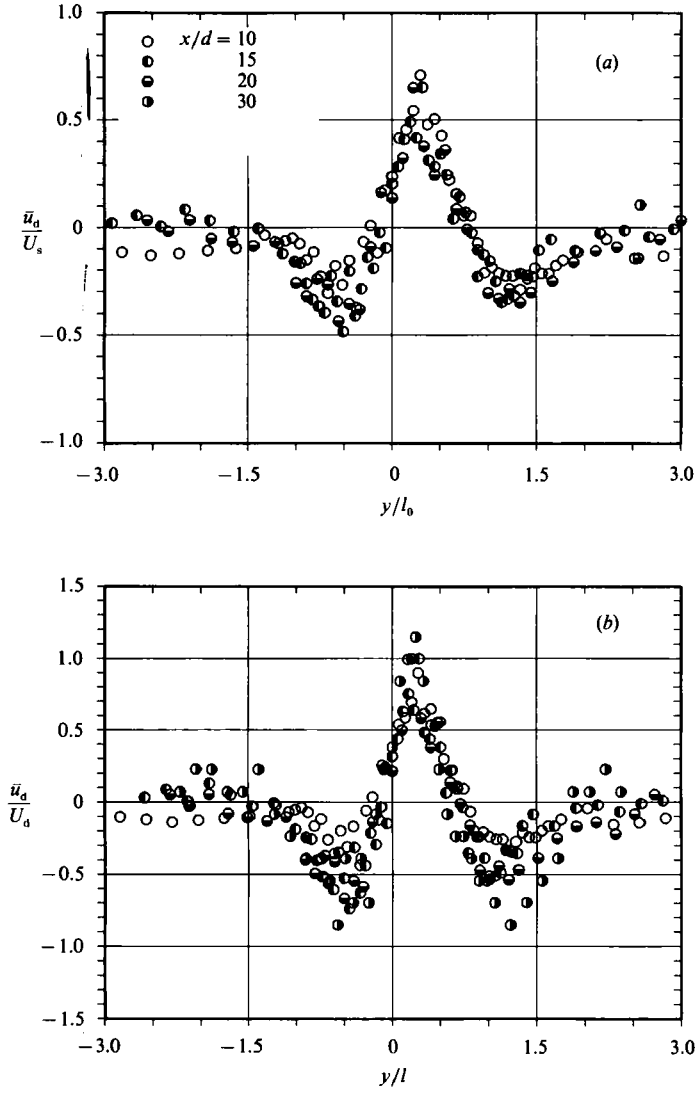

FIGURE 9. Normalized mean velocity profiles for the dual-jet momentumless wake at $Re = 5400$, $x/d = 10$ to 30: normalized by (*a*) l_0 and U_s, and (*b*) l and U_d.

indicating that the flow is highly unsteady. Recall here that we observed a meandering structure in the core region of the dual-jet momentumless wake between the trailing edge and about 5 body diameters downstream in our earlier smoke-wire visualizations (figure 2*c*). This structure became quite irregular at $x/d \approx 5$. Therefore the unsteadiness in the mean velocity measurement of the dual-jet momentumless wake at this particular station is consistent with the flow visualization results.

At streamwise location $x/d = 10$, the peak of the dual-jet momentumless wake is off the model centreline, the profile being nearly symmetric about $y/d = 0.3$. Up to $x/d \approx 5$, the two jets flapped periodically, leading to a symmetric long-time-averaged mean velocity profile; beyond 5 diameters, however, the upper jet became dominant. Minor fluctuations in the experimental set-up may have caused the lower jet to be dominant for brief periods; this can explain the unusual shape of the profile at

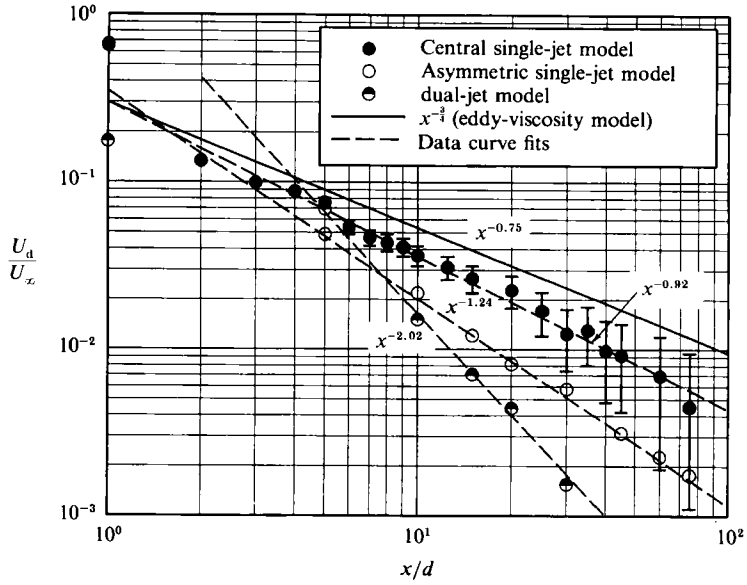

FIGURE 10. Maximum velocity overshoot *vs.* downstream distance for momentumless wakes with different initial conditions at $Re = 5400$. Error bars denote the range of precision in measurements.

$x/d = 5$ and also the larger amount of scatter in all the profiles for this model. The authors took great care to match the two jets as closely as possible. Of course, they could not be matched exactly, and apparently the upper jet was slightly stronger here. Even if the experiment could be improved, the dual jet would probably still eventually jump to asymmetry (although perhaps further downstream than $x/d = 10$), because one of the jets will inevitably dominate in even the most careful experiment. Of the three cases, this dual-jet case was by far the most difficult to set up owing to the complex unsteady interaction between the two jets.

Notice that the maximum velocity overshoot, U_d, of the dual-jet momentumless wake becomes less than 1% of the free-stream velocity as early as $x/d = 20$ while the corresponding downstream locations for the asymmetric single-jet and the central single-jet cases are $x/d = 30$ and 45, respectively (see Park 1989). In other words, the mean velocity profile of the dual-jet momentumless wake flattens out most quickly among the three momentumless wakes considered here.

Because of the centreline shift discussed above, non-dimensional velocity profiles are shown only for $x/d = 10$ to 30 in figure 9. Profiles for far downstream locations such as $x/d = 45$ to 75 were also excluded from this figure because U_d at these stations was extremely small and thus overshadowed by our measurement errors. Similarly to the other two cases, the velocity profiles of the dual-jet case are normalized in two ways: by U_s and l_0 (figure 9*a*), and by U_d and l (figure 9*b*). The quality of normalization with U_s and l_0 is somewhat better than that with U_d and l. Overall, the profiles in both cases are self-similar although there is quite a large scatter.

The decay of maximum velocity overshoot is plotted for the three momentumless wakes on a log-log scale in figure 10. Error bars have been added to the data points of the central single-jet case to denote the range of precision in our measurements; the precision was similar for the other two cases (error bars not shown). For the central single-jet, the asymmetric single-jet and the dual-jet momentumless wakes, the decay laws follow $U_d \sim x^{-0.92}$, $x^{-1.24}$ and $x^{-2.02}$, respectively. No universal decay

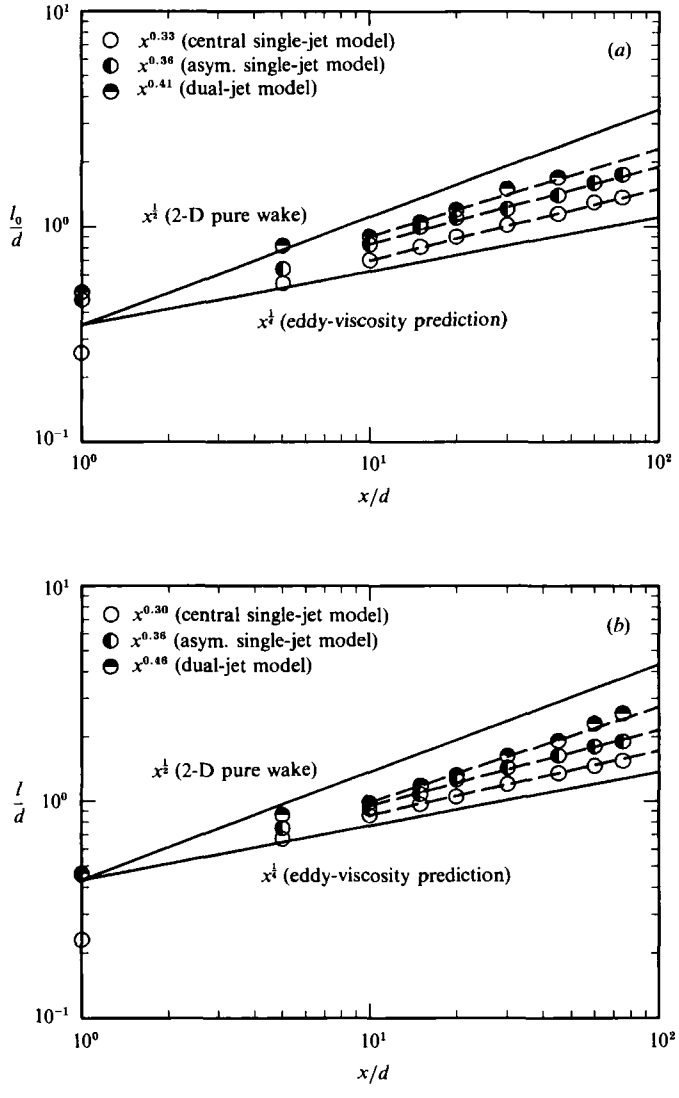

FIGURE 11. Rates of spreading of the momentumless wakes with different initial conditions at $Re = 5400$: (*a*) l_0 (distance between U_{max} and U_{min}), and (*b*) l (half-width of u' profile).

law for U_d seems to exist. Among the three momentumless wakes, the dual-jet case decays more rapidly than the asymmetric single-jet case which in turn decays faster than the central single-jet case.

The spreading rates of the widths l and l_0 for the three momentumless wakes are presented in figure 11. Among the three cases, the central single-jet momentumless wake ($l_0 \sim x^{0.33}$ and $l \sim x^{0.30}$) shows the slowest spreading rate while the dual-jet momentumless wake ($l_0 \sim x^{0.41}$ and $l \sim x^{0.46}$) shows the fastest rate. The asymmetric single-jet case ($l_0 \sim x^{0.36}$ and $l \sim x^{0.36}$) falls between the above two cases.

3.3. *Turbulence measurements*

For the momentumless wake produced by the dual-jet injection model, axial turbulence intensity $(\overline{u'^2})^{\frac{1}{2}}$, transverse turbulence intensity, $(\overline{v'^2})^{\frac{1}{2}}$, and Reynolds stress, $\overline{u'v'}$, were measured with a dual-sensor hot wire at nine streamwise stations

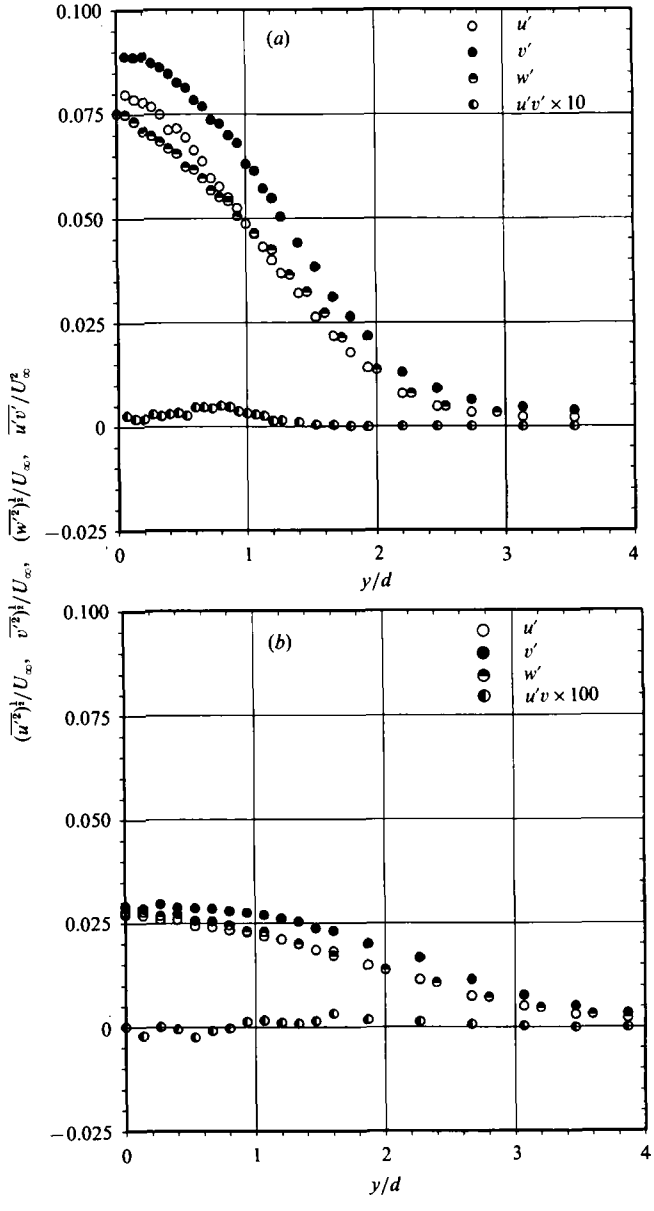

FIGURE 12. Axial, transverse and lateral turbulence intensities and Reynolds stress profiles for the dual-jet momentumless wake at $Re = 5400$: (*a*) $x/d = 15$ and (*b*) $x/d = 45$.

($x/d = 1$ to 75); similar measurements for the central single-jet case were documented in Cimbala & Park (1990). Also, lateral turbulence intensity, $(\overline{w'^2})^{\frac{1}{2}}$, and lateral turbulent shear stress, $\overline{u'w'}$, were measured at streamwise stations 15 and 45 diameters downstream of the model. For the asymmetric single-jet case, only a single hot wire was used; cross-wire surveys were not conducted.

Figure 12(*a*) shows the turbulence intensity profiles at $x/d = 15$ for the dual-jet case. In the early stage ($x/d \leqslant 10$) the flow is strongly anisotropic. Further downstream, however, all three turbulence intensity profiles become Gaussian-like, with the transverse intensity profiles always somewhat higher across the wake

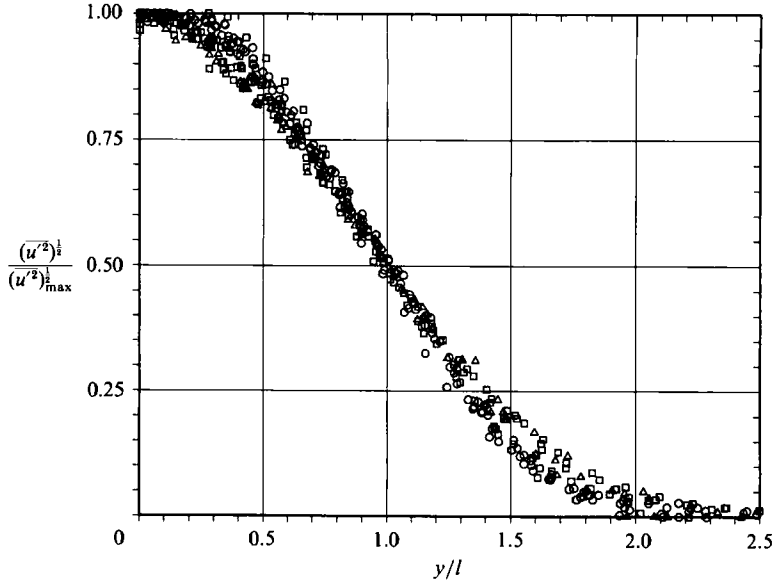

FIGURE 13. Normalized axial turbulence intensity profiles for the momentumless wakes at Re = 5400, x/d = 5 to 75: the central single-jet (○), the asymmetric single-jet (△) and the dual-jet (□) models.

(owing to the flapping). The difference between the peak values of axial intensity and transverse intensity is about 10–12% at $x/d = 15$. The shapes of these profiles are pretty much the same as the central single-jet case, however, their maximum values are about twice as large.

At $x/d = 45$ (figure 12*b*), the turbulence intensity profiles become weaker, but retain basically the same shape. The v' profile, however, becomes somewhat flatter near the centreline, with the maximum transverse turbulence intensity about 7–10% greater than the axial intensity near the centreline. At this downstream location, on the other hand, the lateral $(\overline{w'^2})^{\frac{1}{2}}$ turbulence intensity profiles are almost identical to the axial ones.

The Reynolds stress profiles of the dual-jet case are much different than those of the central single-jet case because of the flapping caused by interaction of the two jets. Because the instantaneous velocity field is not steady nor exactly periodic, overall similarity in the normalized Reynolds stress profiles was not achieved (Park 1989). The Reynolds stress is quite small even by 15 diameters, indicating a rapid return to nearly isotropic turbulence.

Finally, all of the axial turbulence intensity profiles obtained by the three different models (i.e. the central single jet, the asymmetric single jet and the dual-jet injection) are plotted for $x/d = 5$ to 75 in figure 13. The normalized profile appears to be universal for all two-dimensional momentumless wakes generated by different jet-injection models; the shape of the normalized profile is Gaussian-like except for the very near-wake stations, which have not been included in this summary plot. This universality was somewhat unexpected, particularly for the asymmetric jet injection case, whose mean velocity profiles are strongly skewed to one side and thus highly asymmetric. Even for this case the axial turbulence intensity profiles are surprisingly symmetric.

Figure 14 is a summary of the turbulence decay rates for all three models. Both

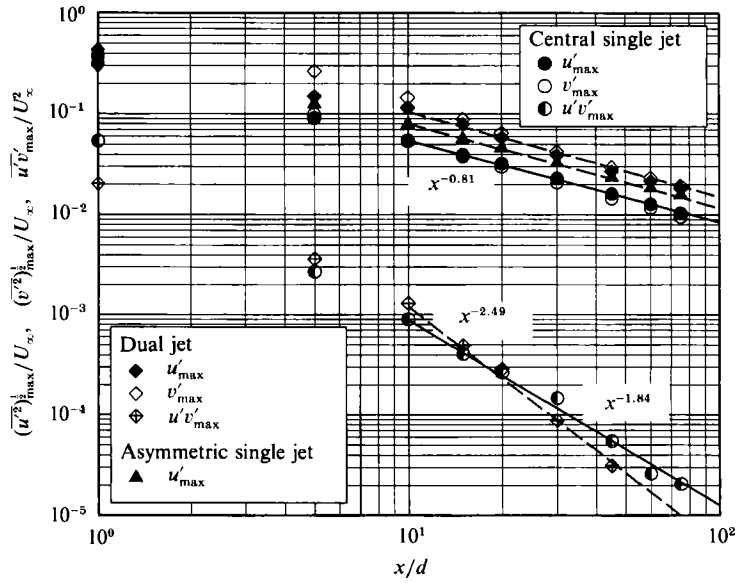

FIGURE 14. Decay of the maximum axial and transverse turbulence intensities and the Reynolds stress for the momentumless wake at $Re = 5400$.

$(\overline{u'^2})^{\frac{1}{2}}_{max}$ and $(\overline{v'^2})^{\frac{1}{2}}_{max}$ for the dual-jet momentumless wake decay as $x^{-0.81}$ beyond $x/d = 10$, which is the same rate as that of the central single-jet momentumless wake. The decay rate of $(\overline{u'^2})^{\frac{1}{2}}_{max}$ for the dual-jet case differs remarkably from that of its maximum mean velocity overshoot, U_d ($x^{-2.02}$). The decay of $\overline{u'v'}_{max}$ for the dual-jet case turns out to follow approximately $x^{-2.49}$. This decay rate is much faster than that of the central single-jet case ($x^{-1.84}$).

For the asymmetric single-jet momentumless wake, the decay rate of $(\overline{u'^2})^{\frac{1}{2}}_{max}$ is again about $x^{-0.81}$. The decay law of the axial turbulence intensity thus also appears to be universal for any different initial conditions as long as the momentumless state is maintained in the flow field.

4. Discussion and conclusions

Experimental study of the two-dimensional momentumless wake produced by three different models has shown that both mean and turbulent quantities exhibit significant dependence on initial conditions (jet injection configuration), even in the far field. Although it was possible in each case to identify appropriate length and velocity scales which normalized the mean velocity profiles into self-similar form, the shape of the normalized profile was determined by the jet configuration. In other words, the momentumless far wake retains a *memory* of its origins, even to the far field.

The rate of decay of maximum velocity overshoot, U_d, was found to be highly dependent on jet injection configuration. In particular, U_d decayed much faster for the dual-jet model ($x^{-2.02}$) than for the central ($x^{-0.92}$) or asymmetric ($x^{-1.24}$) single-jet model. The constant-eddy-viscosity prediction of Tennekes & Lumley (1972) for the two-dimensional momentumless wake ($x^{-0.75}$) far underestimates these experimental results for all three cases. The eddy-viscosity model assumes purely gradient diffusion of turbulence energy; there must therefore exist an additional mechanism

which contributes to the rapid decay of the momentumless wake. One possibility, which was first conjectured by Cimbala & Park (1990), is the ejection of large chunks of turbulent fluid normal to the plane of the wake, caused by mutual induction of vortices of opposite sign. The dual-jet configuration, being more geometrically complex, produces more vortices than the other cases. More turbulent ejections may thus occur, which is consistent with the faster decay rate of the dual-jet momentumless wake. Two such ejections, between 10 and 15 diameters, are visualized in figure 2(*c*).

The axial variation of several mean quantities is listed in table 1 for the present two-dimensional momentumless wakes, as well as for previous axisymmetric cases. Most of the axisymmetric studies involved a central single-jet model; however, Gran (1973) and Schetz & Jakubowski (1975) used models somewhat analogous to the present dual-jet model, namely a propeller-driven and a peripheral-jet injection model respectively. In both cases, U_d was found to decay less rapidly for these peripheral thrust configurations than for the central thrust configurations – opposite to our observations for the two-dimensional case. The reported axisymmetric decay rates are quite diverse, however (from $x^{-0.8}$ to $x^{-2.0}$), and were obtained in different facilities by different techniques; such direct comparisons may not be meaningful.

Various spreading rates of l were also observed for the three different initial conditions in our momentumless wakes. The central single-jet momentumless wake showed the slowest spreading rate ($x^{0.30}$) while the dual-jet momentumless wake showed the fastest ($x^{0.46}$). The asymmetric single-jet case fell between these two ($x^{0.36}$). The constant-eddy-viscosity prediction of Tennekes & Lumley ($x^{0.25}$) again underestimates the experimental results for all three cases. It is interesting to note here that the spreading rate for all three cases falls between the eddy-viscosity prediction for the two-dimensional momentumless wake ($x^{0.25}$) and the theoretically predicted value ($x^{0.50}$) for the pure wake. Compared with pure wakes, entrainment processes near the wake boundaries, which govern the rate of spreading, are not as strong in momentumless wakes owing to the relatively weak mean shear. On the other hand, the eddy-viscosity model does not account for the additional mechanism discussed above; rates of spreading thus fall between these extremes. As seen in table 1, all spreading rates for axisymmetric momentumless wakes fall between the prediction of the constant-eddy-viscosity model ($x^{0.2}$) and the analytical prediction for the axisymmetric pure wake ($x^{0.333}$), which is the same tendency as in the present two-dimensional case.

While U_d and l show significant dependence on initial conditions, the present experiments show that the rate of decay of the axial turbulence intensity is the same for all three models ($x^{-0.81}$), although its magnitude for the dual-jet case is about twice as large as that for the central single-jet case, with the asymmetric single-jet case falling in between. In other words, the decay rate of axial turbulence intensity seems to be universal and independent of initial conditions, even though its magnitude is highly dependent on initial conditions. Furthermore, the normalized u' velocity profiles were nearly identical for all three cases, despite the large differences in mean velocity profiles. From table 1, the decay rate of $(\overline{u'^2})^{\frac{1}{2}}_{\max}$ for the axisymmetric momentumless wakes also seems to be universal (about x^{-1}).

Before concluding this discussion, it may be worth adding a few more comments on initial conditions. Because of the geometrical complexity of momentumless wake generators, there are many lengthscales that may characterize the flow field downstream of the model. For a central single-jet injection model, three possible lengthscales that can be considered are the boundary-layer thickness on the outer

Description and author(s)	U_d	$(\overline{u'^2})^{\frac{1}{2}}_{max}$	$\overline{u'v'}_{max}$	l
Two-dimensional momentumless wakes				
Central-jet (Cimbala & Park 1990)	$x^{-0.92}$	$x^{-0.81}$	$x^{-1.84}$	$x^{0.3}$
Asymmetric single-jet (present)	$x^{-1.24}$	$x^{-0.81}$		$x^{0.36}$
Dual-jet (present)	$x^{-2.02}$	$x^{-0.81}$	$x^{-2.49}$	$x^{0.46}$
Axisymmetric momentumless wakes				
Naudascher (1965)	x^{-2}	x^{-1}	x^{-2} *	$x^{0.2}$
Merritt (1974)				$x^{0.25}$
Lin *et al.* (1973)				$x^{0.25}$
Gran (1973)	$x^{(-0.8)-(-1.4)}$ *	x^{-1} *	$x^{-2.1}$ *	$x^{0.28}$
Higuchi (1977)	$x^{-1.8}$ *	x^{-1} *	$x^{-2.4}$ *	$x^{0.3125}$
Schooley & Stewart (1963)				$x^{0.333}$
Schetz & Jakubowski (1975)**	$x^{-0.969}$	$x^{-0.92}$ *	$x^{-2.7}$ *	
Two-dimensional pure wake				
Chevray & Kovasznay (1969)	$x^{-0.5}$			$x^{0.5}$
Axisymmetric pure wake				
Carmody (1964)	$x^{-0.666}$			$x^{0.333}$
Grid turbulence				
Batchelor (1953)		$x^{-0.5}$		

TABLE 1. Downstream variation of U_d, $(\overline{u'^2})^{\frac{1}{2}}_{max}$, $\overline{u'v'}_{max}$ and l in various wakes. Note that exponents denoted * are approximately interpreted from the original data documented by various authors, and ** denotes the case of a propeller-driven model.

surface of the model, δ, the height of the jet-injection slit, d_j, and the height of the model, d. For a dual-jet injection model, there are even more possible initial variables; four lengthscales that may be considered are δ, d_j, d, and the distance between the two slits, h. We have only begun to explore all the various possible configurations of two-dimensional jet injection models; some other combinations of initial conditions may be explored in future work.

In summary, effects of initial conditions on the momentumless far wake have been examined by changing the method of jet injection. As far downstream as we were able to measure, the decay rate of mean shear and spreading rate were dependent on initial conditions. This implies that the momentumless wake never forgets its origins, and that no single universal pair of exponents for the decay rate of U_d and the spreading rate can be identified for momentumless wakes. On the other hand, the rate of decay of axial turbulence intensity is the same for different initial conditions, even though the magnitude of the turbulence intensity is dependent on initial conditions.

The authors are grateful for the financial support of the Engineering Foundation, USA, under Grant No. RI-A-86-6, and the National Science Foundation, USA, Grant No. MSM-8707653.

REFERENCES

BATCHELOR, G. K. 1953 *The Theory of Homogeneous Turbulence*, pp. 132–138. Cambridge University Press.

CARMODY, T. 1964 Establishment of the wake behind a disk, *Trans. ASME* D: *J. Basic Engng*, **86**, 869–880.

CHEVRAY, R. & KOVASZNAY, L. S. G. 1969 Turbulence measurements in the wake of a thin flat plate. *AIAA J.* **7**, 1641–1643.

CIMBALA, J. M. & PARK, W. J. 1990 An experimental investigation of the turbulent structure in a two-dimensional momentumless wake. *J. Fluid Mech.* **213**, 479–509.

FINSON, M. L. 1975 Similarity behaviour of momentumless turbulent wakes. *J. Fluid Mech.* **71**, 465–479.

GINEVSKII, A. S., POCHKINA, K. A. & UKHANOVA, L. N. 1966 Propagation of turbulent jet flow with zero excess impulse. *Izv. Akad. Nauk. SSSR Mekh. Zhid i Gaza* **1**, 164–166 (English transl. *Fluid Dyn.*, 1967, pp. 106–107).

GRAN, R. L. 1973 An experiment on the wake of a slender propeller-driven body. *Rep.* 20086-6006-RU-00. TRW Systems.

HIGUCHI, H. 1977 Experimental investigation on axisymmetric turbulent wakes with zero momentum defect. Ph.D. thesis, California Inst. of Technology.

LIN, J. T., PAO, Y. H. & VEENHUIZEN, S. D. 1974 Turbulent wake of a propeller-driven slender body in stratified and non-stratified fluids. *Bull Am. Phys. Soc.* **19**, 1165.

MERRITT, G. E. 1974 Wake growth and collapse in stratified flow. *AIAA. J.* **12**, 940–949.

NARASIMHA, R. & PRABHU, A. 1972 Equilibrium and relaxation in turbulent wakes. *J. Fluid Mech.* **54**, 1–17.

NAUDASCHER, E. 1965 Flow in the wake of self-propelled bodies and related sources of turbulence. *J. Fluid Mech.* **22**, 625–656.

PARK, W. J. 1989 An experimental investigation of the turbulent structure in two-dimensional momentumless wakes. Ph.D. thesis, The Pennsylvania State University.

SCHETZ, J. A. & JAKUBOWSKI, A. K. 1975 Experimental studies of the turbulent wake behind self-propelled slender bodies. *AIAA J.* **13**, 1568–1575; also in *AIAA Paper* 75-117, 1975.

SCHOOLEY, A. H. & STEWART, R. W. 1963 Experiments with a self-propelled body submerged in a fluid with a vertical density gradient. *J. Fluid Mech.* **15**, 83–96.

TENNEKES, H. & LUMLEY, J. L. 1972 *A First Course in Turbulence*. MIT Press.